

Nephron organoids derived from human pluripotent stem cells model kidney development and injury

Ryuji Morizane^{1,2}, Albert Q Lam^{1–3}, Benjamin S Freedman^{1,2}, Seiji Kishi^{1,2}, M Todd Valerius^{1–3} & Joseph V Bonventre^{1–3}

Kidney cells and tissues derived from human pluripotent stem cells (hPSCs) may enable organ regeneration, disease modeling and drug screening. We report an efficient, chemically defined protocol for differentiating hPSCs into multipotent nephron progenitor cells (NPCs) that can form nephron-like structures. By recapitulating metanephric kidney development *in vitro*, we generate SIX2⁺SALL1⁺WT1⁺PAX2⁺ NPCs with 90% efficiency within 9 days of differentiation. The NPCs possess the developmental potential of their *in vivo* counterparts and form PAX8⁺LHX1⁺ renal vesicles that self-organize into nephron structures. In both two- and three-dimensional culture, NPCs form kidney organoids containing epithelial nephron-like structures expressing markers of podocytes, proximal tubules, loops of Henle and distal tubules in an organized, continuous arrangement that resembles the nephron *in vivo*. We also show that this organoid culture system can be used to study mechanisms of human kidney development and toxicity.

Chronic kidney disease affects 9–13% of the US adult population and is a serious public health problem worldwide¹. Disease progression is marked by gradual, irreversible loss of nephrons, the individual functional units of the kidney. The ability to generate functional kidney tissue from hPSCs may allow the development of cell therapies for kidney disease as well as strategies for modeling kidney development and disease and for drug screening. Nephrons are made up of glomeruli, which filter the blood plasma into a multicomponent tubular system that reabsorbs and/or secretes solutes and water to produce urine. The many different epithelial cell types in nephrons have complicated efforts to generate them *in vitro*. However, studies have shown that all of these epithelial cell types except those in the collecting ducts derive from a multipotent NPC population present in the metanephric cap mesenchyme during kidney development^{2–5}. The NPCs, which express the markers SIX2, SALL1, WT1 and PAX2, are found in humans only during kidney organogenesis, which ceases by birth and cannot be reinitiated after birth, even during repair after kidney injury^{6,7}. However, these NPC markers are also expressed in the more primitive mesonephric mesenchyme that derives from the anterior intermediate mesoderm and forms the transiently functional mesonephros⁸. This suggests that careful attention to the early separation of anterior versus posterior intermediate mesoderm fate is likely to be critical for the proper induction of metanephric NPCs (*Supplementary Fig. 1a*).

Several studies have attempted to differentiate mouse and human PSCs into cells of the kidney lineage^{9–19}. Published protocols to produce SIX2⁺ NPCs from hPSCs^{17–21} have several limitations. First, differentiation efficiency is too low for large-scale production of NPCs. One explanation

for this may be that most protocols have not distinguished anterior from posterior intermediate mesoderm in early steps of directed differentiation. The metanephric mesenchyme derives from cells of the primitive streak, which persist as cells of the posterior intermediate mesoderm¹⁷. In contrast the ureteric bud, the precursor to the adult kidney collecting duct system, originates in the anterior intermediate mesoderm, a cell population incapable of giving rise to the metanephric mesenchyme^{22,23}. Second, existing protocols use poorly defined components, such as mouse embryonic spinal cord¹⁷, which would not be suitable for clinical applications. Finally, previous studies have generated nephron rudiments^{17,18} but not mature nephron segments containing the mature kidney epithelial cell types or a single contiguous nephron-like structure with characteristics of multiple nephron segments, precluding their use for modeling human kidney development, disease and injury.

Here we describe an efficient, chemically defined system for differentiating hPSCs into multipotent NPCs capable of forming nephron-like structures. By carefully recapitulating the stages of metanephric kidney development in two-dimensional (2D) monolayer culture, we generate NPCs that co-express the critical markers SIX2, SALL1, WT1 and PAX2 with 90% efficiency within 9 days of initiation of differentiation—a substantial improvement over previous methods (*Supplementary Fig. 1b*). The NPCs can spontaneously form PAX8⁺LHX1⁺ renal vesicles that differentiate further into several epithelial nephron structures. This process can be markedly enhanced by mimicking *in vivo* nephron induction by transiently treating the NPCs with the GSK-3β inhibitor CHIR99021 (CHIR) and FGF9 to induce renal vesicle formation. This is followed by self-organizing differentiation into continuous structures

¹Renal Division, Department of Medicine, Brigham and Women's Hospital, Boston, Massachusetts, USA. ²Department of Medicine, Harvard Medical School, Boston, Massachusetts, USA. ³Harvard Stem Cell Institute, Cambridge, Massachusetts, USA. Correspondence should be addressed to R.M. (morizanr@da2.so-net.ne.jp) or J.V.B. (jbonventre@partners.org).

Received 9 June; accepted 6 October; published online 12 October 2015; doi:10.1038/nbt.3392

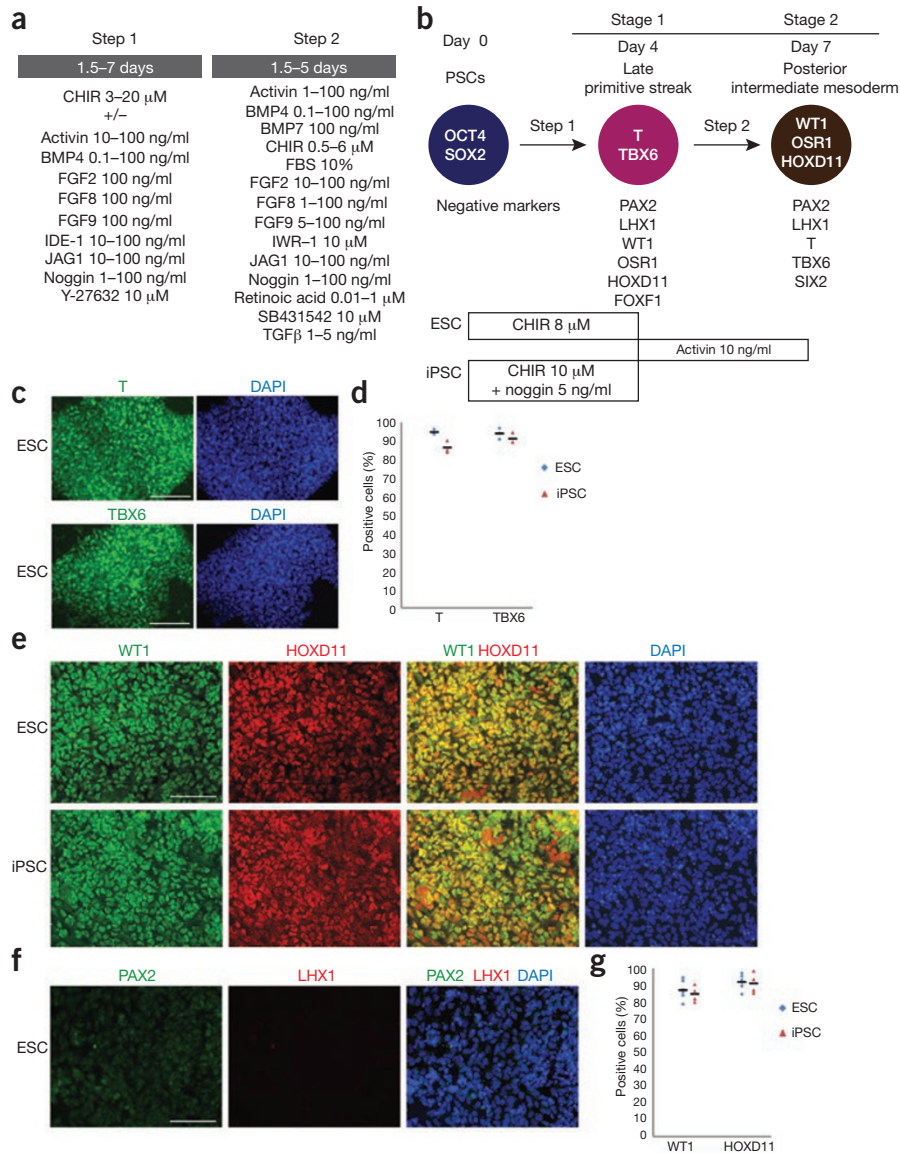


Figure 1 Differentiation of hPSCs into posterior intermediate mesoderm. **(a)** Agents that were tested for the induction of late primitive streak and posterior intermediate mesoderm (IM). **(b)** Diagram and the protocol of differentiation of hPSCs sequentially into late primitive streak and posterior intermediate mesoderm (IM) with markers identifying both states by their presence or absence. In the protocol for posterior IM hESCs and hiPSCs were differentiated with CHIR 8 μ M and 10 μ M, respectively. For hiPSCs noggin 5 ng/ml was also required. **(c)** Immunocytochemistry for T and TBX6 in hESCs on day 4 of the differentiation with CHIR 8 μ M. Scale bars (**c,e,f**), 100 μ m. **(d)** Percentage of T⁺ or TBX6⁺ cells in hESCs and hiPSCs on day 4. Black bars indicate mean values. $n = 3$ for hESCs; $n = 3$ for hiPSCs. **(e)** Immunocytochemistry for WT1 and HOXD11, posterior IM markers, in hESCs and hiPSCs on day 7. **(f)** Immunocytochemistry for PAX2 and LHX1, anterior IM markers in hESCs on day 7. **(g)** Percentage of WT1⁺ or HOXD11⁺ cells in hESCs and hiPSCs on day 7. Black bars indicate mean values. $n = 7$ for hESCs; $n = 4$ for hiPSCs.

with sequential characteristics of podocytes, proximal tubules, loops of Henle and distal tubules in both 2D and three-dimensional (3D) culture.

RESULTS

Efficient induction of posterior intermediate mesoderm

Recent efforts to direct the differentiation of PSCs into cells of the kidney lineage have focused the first step of differentiation on induction of the posterior primitive streak using a combination of growth factors that includes BMP4 (refs. 17,18). The inclusion of BMP4 is justified by

evidence that a gradient of Wnt3a and BMP4 patterns the anterior-posterior axis of the mouse primitive streak^{24,25}. However, recent developmental studies on early mesoderm patterning led us to reconsider this rationale. First, cells originating in the posterior primitive streak give rise to lateral plate mesoderm and not intermediate mesoderm, from which the kidneys are derived (**Supplementary Fig. 2a**)²⁶. Second, the timing of migration of mesodermal precursors out of the primitive streak determines mesodermal patterning along the anterior-posterior axis²⁷. Thus, precursor cells of the more anterior mesoderm migrate out of the primitive streak earlier than those of posterior mesoderm. We therefore hypothesized that the embryonic origin of the posterior intermediate mesoderm was not the cells of the posterior primitive streak but rather cells of the late-stage primitive streak, and that precisely recapitulating the developmental pathway defining both the anterior-posterior position along the primitive streak as well as the timing of migration out of the primitive streak would optimize the differentiation of PSCs into posterior intermediate mesoderm.

To test this hypothesis, we treated human embryonic stem cells (hESCs; line H9) with varying doses and durations of CHIR, which we and others previously showed could effectively differentiate hPSCs into T⁺ primitive streak^{17,18,20}, solely or in combination with multiple developmental growth factors and small-molecule inhibitors of developmental signaling pathways (**Fig. 1a,b**). High-dose CHIR (8 μ M) over 4 days robustly induced and maintained a population of T⁺TBX6⁺ primitive streak cells (**Fig. 1b-d** and **Supplementary Fig. 2b-d**). Subsequent treatment with activin (10 ng/ml) between days 4 and 7 successfully induced WT1⁺HOXD11⁺PAX2⁻LHX1⁻ cells with nearly 90% efficiency, whereas WT1⁺HOXD11⁻ cells were induced without activin (**Fig. 1e-g** and **Supplementary Fig. 2e**). PAX2 and LHX1 were not expressed (**Fig. 1f**), confirming that activin treatment of late primitive streak cells produced posterior and not anterior intermediate mesoderm cells^{8,17}. Moreover, shortening or extending CHIR treatment did not efficiently induce WT1⁺HOXD11⁺ cells after subsequent activin treatment, indicating that 4 days of CHIR treat-

ment was optimal for efficient induction of late primitive streak and then posterior intermediate mesoderm.

To determine the reproducibility of posterior intermediate mesoderm induction in other hPSC lines, we next tested the combination of high-dose CHIR with activin, BMP4, FGF2, FGF8, FGF9, IDE-1, JAG1, noggin or Y-27632 for 4 days followed by treatment with activin in HDF- α human induced (hi)PSCs²⁰. Intrinsic differences between HDF- α hiPSCs and H9 ESCs^{28,29} mandated slight modifications to the protocol to optimize the production of posterior intermediate meso-

derm cells. HDF- α hiPSCs required a higher dose of CHIR ($10\ \mu\text{M}$) to induce T $^+$ TBX6 $^+$ primitive streak with an efficiency similar to that of H9 hESCs (Supplementary Fig. 3a). When HDF- α hiPSCs treated with CHIR $10\ \mu\text{M}$ for 4 days were then treated with activin for 3 days, HOXD11, but not WT1, was expressed on day 7 (Supplementary Fig. 3e). The absence of WT1 suggested a failure of these factors to induce posterior intermediate mesoderm in hiPSCs. To determine whether other posterior mesoderm subtypes had been induced by our differentiation protocol, we immunostained H9 hESCs and HDF- α hiPSCs on day 4 following treatment with CHIR. The hiPSCs but not the hESCs expressed FOXF1, a marker of the posterior primitive streak and lateral plate mesoderm³⁰ (Supplementary Fig. 3b).

As the posterior primitive streak is induced by a BMP4 signal gradient^{24,30}, we hypothesized that CHIR treatment of HDF- α hiPSCs might induce endogenous BMP4 production that promotes differentiation into the posterior primitive streak and, subsequently, the lateral plate mesoderm. The addition of low-dose noggin ($5\ \text{ng}/\text{ml}$), a BMP4 signaling antagonist³¹, with CHIR in the first step of differentiation suppressed BMP4 to an optimal level to yield cells that expressed T and TBX6 but

not FOXF1 on day 4 (Supplementary Fig. 3c). Subsequent differentiation with activin resulted in the generation of WT1 $^+$ HOXD11 $^+$ posterior intermediate mesoderm cells with 80–90% efficiency (Fig. 1b–g and Supplementary Fig. 3e). Although H9 hESCs did not express FOXF1 on day 4 in response to CHIR, the addition of low concentrations of BMP4 ($1\ \text{ng}/\text{ml}$) resulted in FOXF1 expression at day 4 and suppression of WT1 expression on day 7, similar to what we observed in the hiPSC line (Supplementary Fig. 3d). Collectively, these results show that the efficacy of posterior intermediate mesoderm induction was highly sensitive to the presence of BMP4 signaling at the primitive streak stage in hiPSCs. Optimizing the protocol for individual cell lines based on their endogenous BMP4 production maximized the efficiency of generating posterior intermediate mesoderm.

Induction of multipotent nephron progenitor cells

To differentiate WT1 $^+$ HOXD11 $^+$ posterior intermediate mesoderm cells into NPCs of the metanephric mesenchyme, we treated them on day 7 with varying doses of FGF9 (5 – $200\ \text{ng}/\text{ml}$), which we and others have previously shown to induce SIX2 $^+$ cells^{17,18,20,32}. A low

dose of FGF9 ($10\ \text{ng}/\text{ml}$) was sufficient to induce SIX2 $^+$ cells with an efficiency of 90% within 1–2 days of treatment (Fig. 2a,b). These SIX2 $^+$ cells co-expressed other critical markers of the NPCs of the metanephric mesenchyme, including SALL1, WT1, PAX2 and EYA1 (Fig. 2b–d), as assessed by immunocytochemistry and flow cytometry. We therefore considered these SIX2 $^+$ SALL1 $^+$ WT1 $^+$ PAX2 $^+$ cells to be putative NPCs. Though we were unable to assay OSR1 expression by immunostaining owing to the lack of highly specific antibodies, we could detect high levels of OSR1 transcript as early as day 7 (posterior intermediate mesoderm) and sustained through day 9 (NPCs) by quantitative real-time PCR (Fig. 2e). SIX2 expression in these cells could be sustained for at least 1 week with continuous exposure to FGF9 (Fig. 2f,g).

Even with continuous FGF9 treatment, we observed that between days 10 and 14 of differentiation some of the NPCs spontaneously downregulated SIX2 expression and differentiated into round, polarized clusters of PAX8 $^+$ LHX1 $^+$ cells reminiscent of renal vesicles (Fig. 2f,g and Supplementary Fig. 4a)³³.

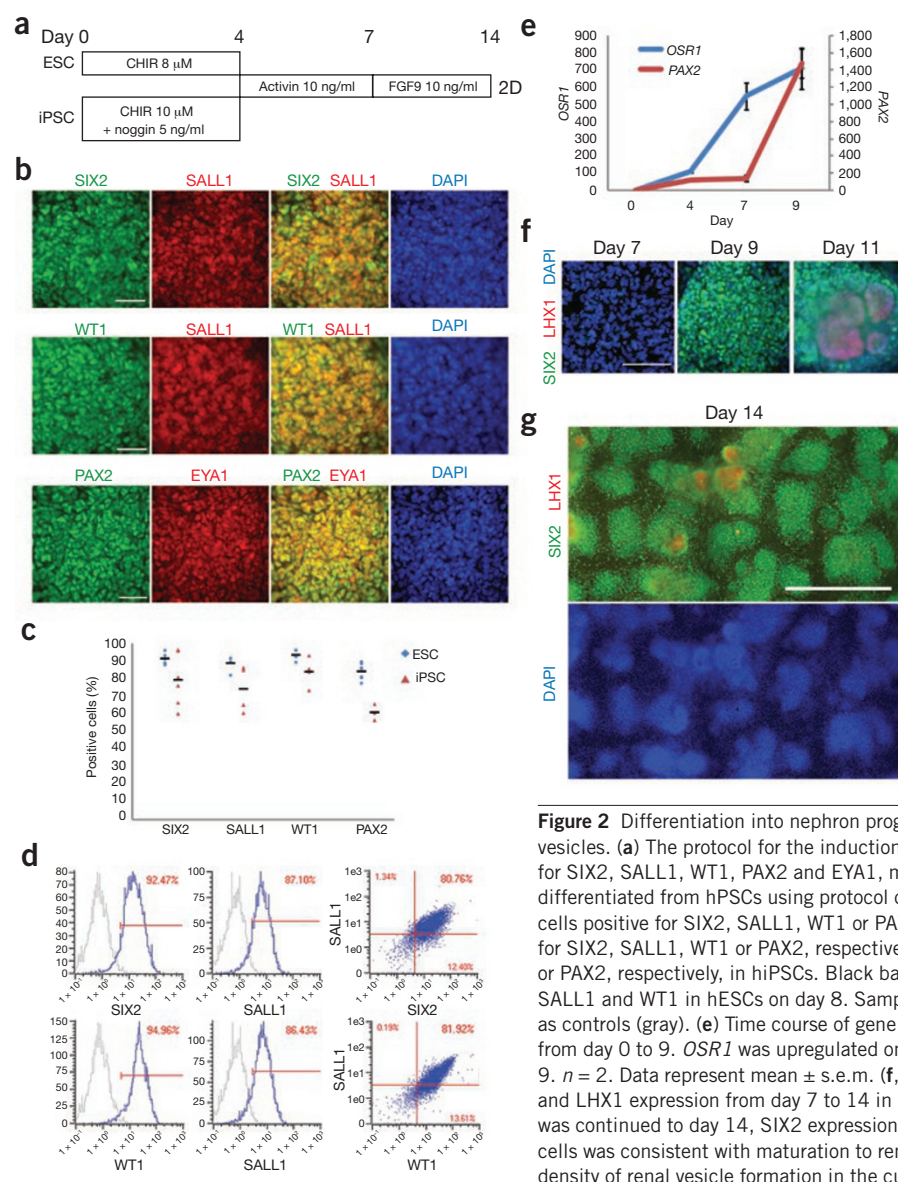


Figure 2 Differentiation into nephron progenitor cells and spontaneous formation of renal vesicles. (a) The protocol for the induction of nephron progenitor cells. (b) Immunocytochemistry for SIX2, SALL1, WT1, PAX2 and EYA1, markers of nephron progenitor cells, on day 9 in cells differentiated from hPSCs using protocol depicted in a. Scale bars, $50\ \mu\text{m}$. (c) Percentage of cells positive for SIX2, SALL1, WT1 or PAX2 in hESCs and hiPSCs on day 9. $n = 7, 5, 4$ or 7 for SIX2, SALL1, WT1 or PAX2, respectively, in hESCs. $n = 6, 4, 4$ or 3 for SIX2, SALL1, WT1 or PAX2, respectively, in hiPSCs. Black bars indicate mean values. (d) Flow cytometry for SIX2, SALL1 and WT1 in hESCs on day 8. Samples stained with secondary antibodies alone were used as controls (gray). (e) Time course of gene expression of OSR1 and PAX2 in hESCs by qRT-PCR from day 0 to 9. OSR1 was upregulated on days 7 and 9 whereas PAX2 was upregulated on day 9. $n = 2$. Data represent mean \pm s.e.m. (f,g) Immunocytochemistry shows time course of SIX2 and LHX1 expression from day 7 to 14 in hESCs treated with FGF9 10 ng/ml. (g) When FGF9 was continued to day 14, SIX2 expression was sustained, but spontaneous induction of LHX1 $^+$ cells was consistent with maturation to renal vesicles. The images are representative of the density of renal vesicle formation in the culture dishes. Scale bars, $100\ \mu\text{m}$ (f), 1 mm (g).

Upon withdrawal of FGF9 on day 10, these renal vesicle-like clusters proceeded to expand and elongate into tubular structures, resembling the process of nephron formation *in vivo* (**Supplementary Fig. 4b**). Immunocytochemistry of the elongated structures revealed that they contained *Lotus tetragonolobus lectin* (LTL)⁺N-cadherin (CDH2)⁺ and nephrin (NPHS1)⁺podocalyxin (PODXL)⁺ cells reminiscent of proximal tubules and podocytes, respectively (**Supplementary Fig. 4c**). Thus, in the absence of exogenous signals after day 10, hPSC-derived NPCs are intrinsically programmed to differentiate into early-stage epithelial structures of the nephron.

To test whether the formation of epithelial structures could be facilitated by 3D culture conditions, on day 10, at the time of FGF9 withdrawal, we replated NPCs in ultra-low-attachment, round-bottom, 96-well plates and cultured them for 1 week. NPCs formed 3D spherical aggregates, one per well, in suspension culture. Whole-mount staining of aggregates at day 16 revealed the presence of LTL⁺ tubules and clusters of NPHS1⁺PODXL⁺WT1⁺ cells (**Supplementary Fig. 4g,h**). Co-culturing NPCs in 3D with Wnt4-expressing NIH3T3 mouse embryonic fibroblast cells³⁴ or a ureteric bud cell line³⁵ did not significantly increase the LTL⁺ tubules in organoids (**Supplementary Fig. 4d-f**), in contrast to a previous report¹⁷. Similarly, the addition of six growth factors (BMP7, HGF, IGF-1, JAG1, WNT4 and mouse Wnt9b) or three small molecules (CHIR, IWR-1, SB431542) did not significantly increase the number of LTL⁺ tubules (**Supplementary Fig. 4e**). These results suggested the need for more accurate recreation of temporal signal activation.

Spontaneous morphogenesis into nephron structures

Although we observed spontaneous differentiation of SIX2⁺ NPCs into PAX8⁺LHX1⁺ renal vesicles and early nephron epithelia in both 2D and 3D culture, the efficiency of this process was relatively low. During mouse

nephrogenesis, Wnt9b, secreted by the ureteric bud, induces the metanephric cap mesenchyme to undergo a mesenchymal-to-epithelial transition by upregulation of Wnt4 in nephron progenitors³⁶, and the inductive Wnt signals are subsequently suppressed during formation of renal vesicles, possibly by Dkk1 (ref. 37). This induction can be mimicked *ex vivo* or *in vitro* by the transient treatment of isolated mouse metanephric mesenchyme or fluorescence-activated cell-sorted SIX2⁺ cells with the GSK-3β inhibitor BIO³⁸. We therefore sought to improve the efficiency of generating renal vesicles through transient rather than sustained activation of Wnt signaling in NPCs. Through a systematic screen of growth factors and small molecules, including CHIR (**Supplementary Fig. 5a,b**), in 2D cultures, we found that treating NPCs with low-dose CHIR (3 μM) for 2 days from day 9 while simultaneously maintaining exogenous FGF9 signaling (days 7–14) markedly increased the number of cells that downregulated SIX2 and co-expressed PAX8 and LHX1 (**Fig. 3a-c** and **Supplementary Fig. 5c**). Quantification by flow cytometry revealed that 76% of differentiated cells were PAX8⁺LHX1⁺ (**Fig. 3d**). PAX8⁺LHX1⁺ cells were organized in laminin-bound, polarized round clusters morphologically resembling renal vesicles *in vivo* (**Fig. 3e**). The cells also expressed HNF1β and BRN1, the other markers of renal vesicles, suggesting that they represented renal vesicles (**Fig. 3e**). In 3D culture from day 9, the same treatment with CHIR and FGF9

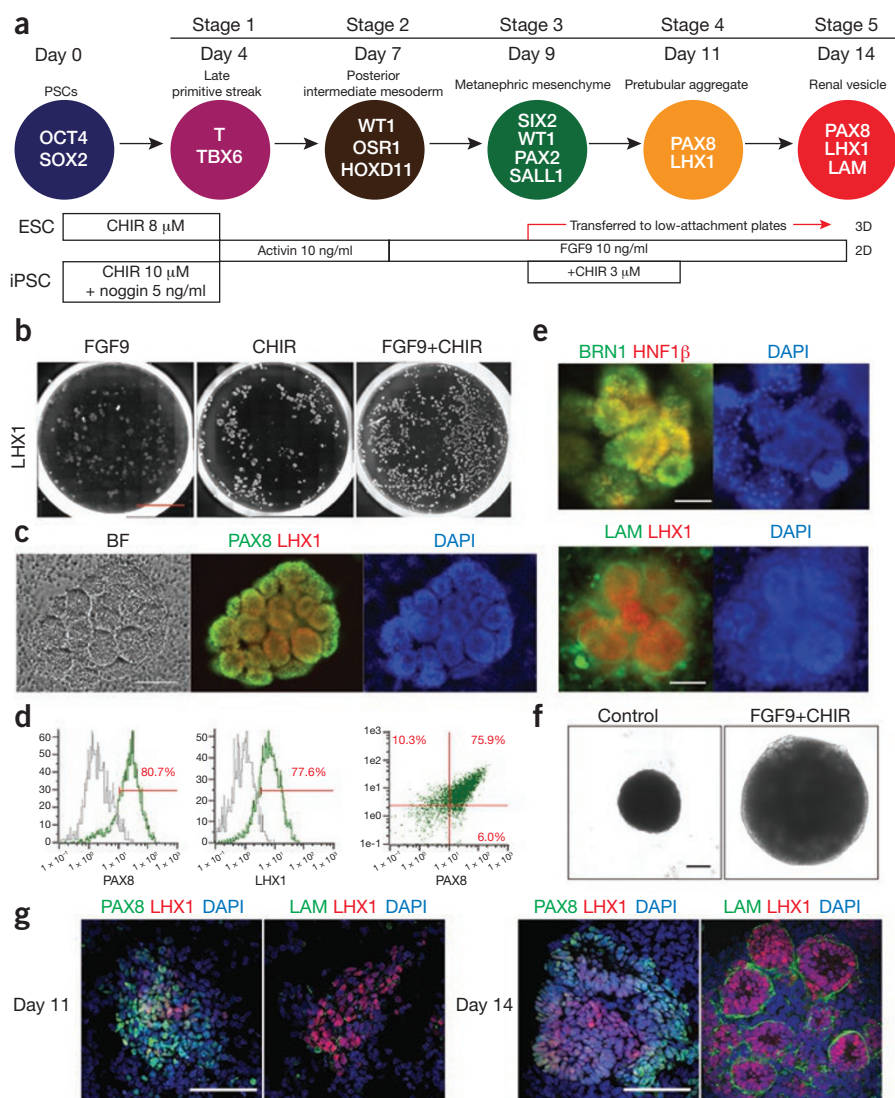


Figure 3 Induction of pretubular aggregates and renal vesicles from nephron progenitor cells. (a) Diagram of differentiation into renal vesicles. (b) Whole-well scan for LHX1 in 24-well plate on day 14 of differentiation. The combination of FGF9 10 ng/ml and transient CHIR 3 μM treatment enhanced LHX1 expression. *n* = 2. Scale bar, 5 mm. (c) Representative images of brightfield and immunocytochemistry for PAX8 and LHX1 in hESCs on day 14. Scale bar, 100 μm. (d) Flow cytometry for PAX8 and LHX1 in hESCs on day 14. Samples treated with secondary antibodies alone were used as controls (gray). (e) Immunocytochemistry for BRN1, HNF1β and LAM (laminin) on day 14 of differentiation. *n* = 6. Scale bars, 100 μm (upper), 50 μm (lower). (f) Bright-field imaging of the organoids that formed in culture after cells were resuspended on day 9, transferred to ultra-low-attachment 96-well plates and studied on day 14. Controls were cultured in the basic differentiation medium (ARPMI) after resuspension. FGF9 and CHIR increased the size of the organoids. Scale bar, 100 μm. (g) Whole-mount staining of the organoids on day 11 and 14. Polarized structures surrounded by laminin were found on day 14, suggesting the differentiation into renal vesicles. *n* = 2. Scale bars, 100 μm.

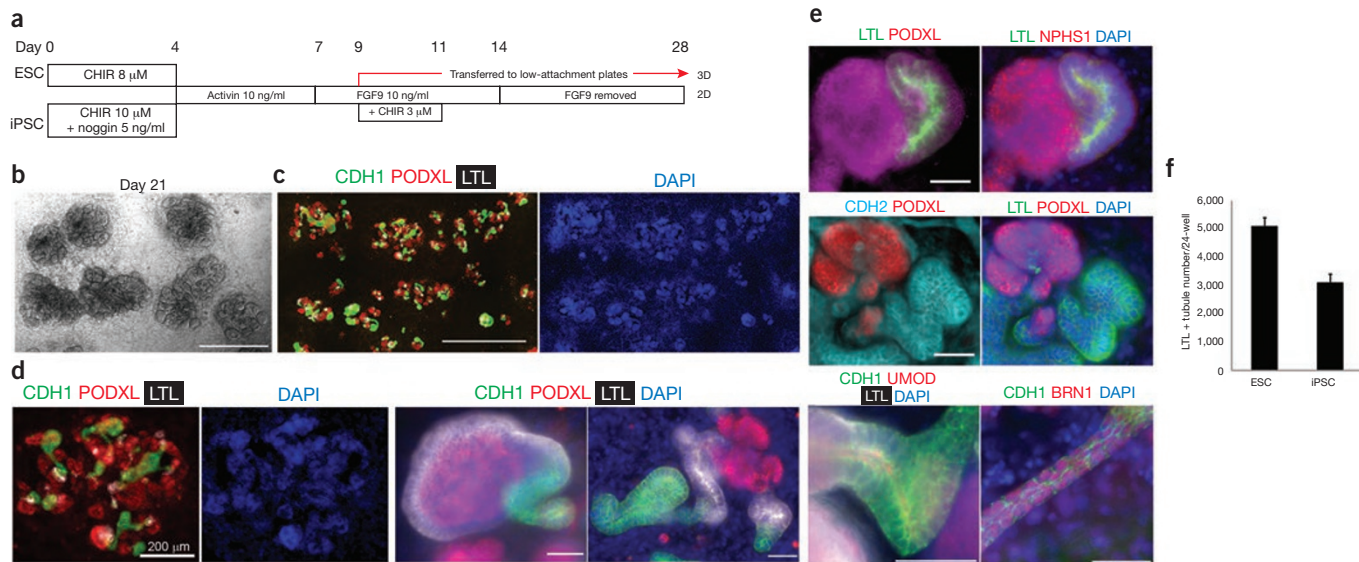


Figure 4 Self-organizing nephron formation in 2D culture. (a) The protocol for the induction of nephrons. (b) Representative bright-field images on day 21 of differentiation. Scale bar, 1 mm. (c,d) Immunocytochemistry for CDH1, PODXL and LTL on day 21. (c) Low magnification. Scale bar, 1 mm. (d) High magnification. Scale bar, 50 μ m, unless otherwise indicated. (e) Immunocytochemistry for podocyte (PODXL, NPHS1) proximal tubule (CDH2, LTL), loop of Henle (CDH1, UMOD) and distal tubule (CDH1, BRN1) markers on days 21–28. $n = 7$. Scale bars, 50 μ m, unless otherwise indicated. (f) The number of LTL⁺ tubules in structures derived from hESCs and hiPSCs on day 21; $n = 2$. Values were calculated from ten fields (1 mm²/field) in each sample. Data represent mean \pm s.e.m.

induced similar structures: PAX8⁺LHX1⁺LAM⁻ pretubular aggregates and PAX8⁺LHX1⁺LAM⁺ renal vesicles became apparent on day 11 and 14, respectively, and grew larger over time (Fig. 3f,g).

By day 21 of differentiation, the renal vesicles spontaneously formed elongated epithelial nephron structures without additional factors (Fig. 4a–c). These structures expressed segmental markers of the nephron in a contiguous arrangement, including glomerular podocytes (NPHS1⁺PODXL⁺), proximal tubules (LTL⁺CDH2⁺) and loops of Henle/distal tubules (E-cadherin (CDH1)⁺uromodulin (UMOD)⁺BRN1⁺) (Fig. 4c–e)^{39–41}. Nephron-like structures were generated by day 21 of differentiation, with an efficiency >20 times greater than that of our previous protocol (Fig. 4f)²⁰, and could be sustained until at least day 56. No outgrowth of collecting duct (CDH1⁺Dolichos biflorus agglutinin (DBA)⁺) structures, which are derived from the ureteric bud and not the metanephric mesenchyme, from renal vesicles was seen, confirming that our differentiation protocol was specific for producing NPCs of the metanephric mesenchyme.

Generation of *in vitro* kidney organoids in 3D culture

Next we investigated whether a 3D culture environment could promote the formation of more organized nephron structures with tubules possessing a lumen. We replated cells cultured in 2D on days 9, 11 and 14 corresponding to NPCs, pretubular aggregates and renal vesicles, respectively, into 3D suspension culture and applied the same protocol as with 2D (Fig. 4a). Replating day 9 cultures showed the greatest induction of nephron-like structures. Whole-mount immunostaining of organoids from days 21–35 of differentiation revealed numerous contiguous nephron-like structures with features of nephron segments from glomerulus to distal tubule (Fig. 5a–c). Clusters of podocyte-like cells (NPHS1⁺PODXL⁺WT1⁺) were surrounded by Bowman's capsule-like structures, connected to tubular structures with markers of proximal tubules (LTL⁺AQP1⁺), descending limbs of Henle (CDH1⁺AQP1⁺), thick ascending limbs of Henle (CDH1⁺UMOD⁺) and distal convoluted tubules (CDH1⁺UMOD⁻) expressed in the same sequence as in the

in vivo nephron (Fig. 5d)^{39,41}. SIX2 expression was absent in 3D kidney organoids, suggesting that NPCs had completely differentiated into nephron epithelia. Furthermore, the expression of SALL1, another NPC marker that is transiently expressed in immature nephron tubules, was not detected in nephron-like structures, indicating that these structures were more mature than those in prior reports¹⁷. Characterization of the nonepithelial cells comprising the interstitial compartment between nephron-like structures revealed that these cells were negative for the metanephric stromal progenitor marker FOXD1, the endothelial marker endomucin and the fibroblast marker α -smooth muscle actin, indicating that these cell types did not constitute a significant cell population within the organoids (data not shown).

Electron microscopy of the kidney organoids at day 21 of differentiation revealed ultrastructural features characteristic of mature renal epithelia. Structures resembling foot processes were noted on the surface of podocyte-like cells, which were encapsulated by a layer of cells reminiscent of Bowman's capsule (Fig. 5e,f, upper panels). Tubular structures possessed a discrete lumen and epithelial tight junctions similar to kidney tubules, and a subset of the tubules contained mitochondria-rich cells with brush border-like structures, characteristic features of proximal tubular cells (Fig. 5e,f, lower panels). These findings demonstrate that differentiation of the NPCs in suspension culture results in the formation of 3D kidney organoids and organized, multicomponent nephron-like structures with distinct lumens in a contiguous and sequential arrangement that mimics the nephron.

Modeling kidney development and toxicity with organoids

The observation that no additional exogenous chemicals are required for hPSC-derived renal vesicles to form more mature nephron structures indicated that the signals for nephron formation are endogenously activated after renal vesicles are formed. As patterning of the nephron into its different segments begins at the renal vesicle stage during development⁴², we postulated that developmental patterning could be mimicked by chemical modulation of these endogenous signals. Addition of

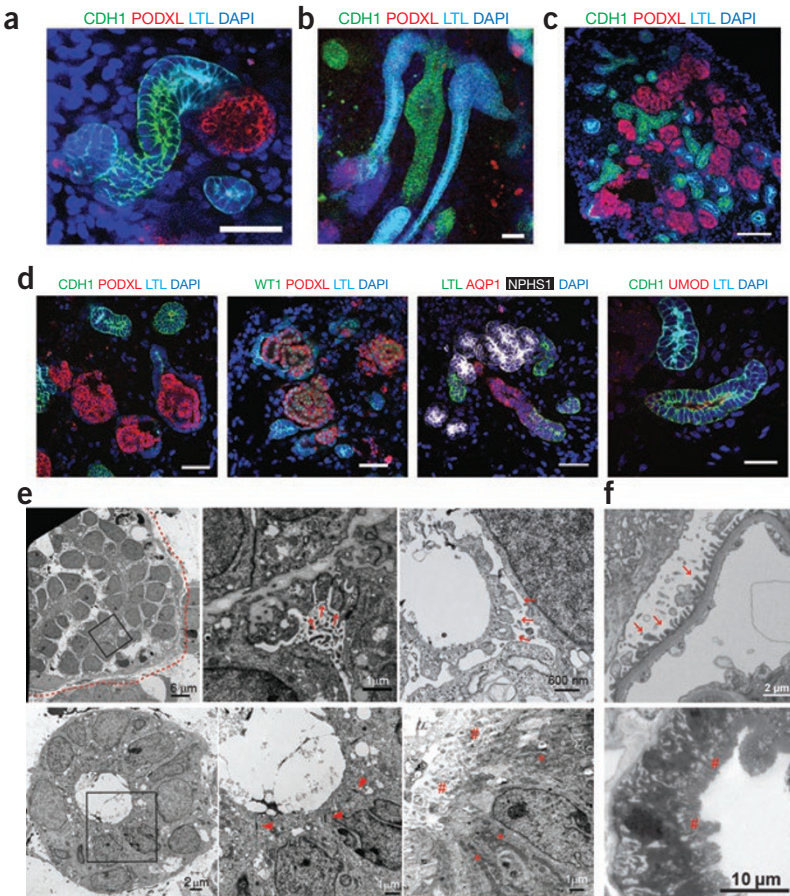


Figure 5 Self-organizing nephron formation in 3D culture. (a,b) Whole-mount staining for CDH1, PODXL and LTL on day 28 (a) and 35 (b) using protocol in **Figure 4a**. Scale bar, 50 μ m. (c,d) Representative immunohistochemistry in structures derived from hESCs and hiPSCs on day 21–28. $n = 5$. Scale bars, 50 μ m. AQP1: aquaporin1. (e) Low magnification. (d) High magnification. (e) Representative electron microscopy images of glomerulus-like and tubule regions of kidney organoids derived from hESCs. Middle panels are higher magnification enlargement of the square-enclosed regions within left panels. $n = 5$. Samples were taken at 21 days with the exception of the top right panel, which was taken at day 18 and did not have transient CHIR treatment. Dotted lines: Bowman's capsule. Arrows: foot process. Arrow heads: tight-junction. Asterisks: mitochondria. Hashes: brush border-like structures. (f) Electron microscopy images of normal human kidneys showing foot processes (upper panel) and brush borders (lower panel).

the Notch signaling inhibitor DAPT from day 14 to 21 of differentiation resulted in a marked suppression of proximal tubule formation in both 2D and 3D culture (**Fig. 6a,b** and **Supplementary Fig. 6a–c**), consistent with previous studies implicating Notch signaling in proximal patterning of the nephron^{43,44}.

Drug nephrotoxicity is an important cause of acute kidney injury in hospitalized patients⁴⁵. Currently there are no patient-specific models to assay nephrotoxicity *in vitro*. To test whether our organoids could be used to study kidney injury and toxicity *in vitro*, we treated 3D hESC-derived kidney organoids after 21 days of differentiation for 48 h with gentamicin (5 mg/ml), a commonly used antibiotic with well-established proximal tubular toxicity⁴⁶, or for 24 h with cisplatin (5 μ M), an anticancer drug with proximal and distal tubular toxicity. Organoids were then fixed and immunostained for kidney injury molecule-1 (KIM-1), a biomarker that is highly upregulated in the proximal tubules after acute kidney injury⁴⁷, together with LTL and E-cadherin to identify proximal and distal tubules, respectively.

Staining of both whole mount and frozen sections of gentamicin-treated organoids demonstrated clear KIM-1 expression at the luminal

surface of LTL⁺ tubules but not in E-cadherin⁺ tubules, and real-time PCR showed KIM-1 upregulation by gentamicin in a dose-dependent manner (**Fig. 6c–e** and **Supplementary Fig. 7a,b**), indicating that gentamicin had injured proximal tubules in the organoids. Moreover, cisplatin significantly ($P = 0.006$; control vs. 5 mg/ml) upregulated KIM-1 in LTL⁺ tubules and suppressed E-cadherin expression (**Fig. 6c**), indicating proximal and distal tubular toxicity. No KIM-1 expression was observed in either LTL⁺ or E-cadherin⁺ tubules in untreated organoids. To distinguish between a generalized toxic effect and nephron segment-specific injury, the organoids were immunostained for γ H2AX, a marker of DNA damage (**Fig. 6f**). Cisplatin at a dose of 5 μ M upregulated γ H2AX expression in LTL⁺ tubules but not in PODXL⁺ podocytes, whereas a higher dose of cisplatin (50 μ M) resulted in more widespread γ H2AX expression, consistent with more generalized cell toxicity. These findings establish the utility of our 3D kidney organoid system as a patient-specific model of toxic kidney injury that can be employed to test the nephrotoxicity of drugs and other chemicals *in vitro*.

DISCUSSION

We describe the generation of segmentally patterned nephron structures from hPSCs by directed differentiation. Our protocol efficiently induces NPCs that spontaneously form renal vesicles in both 2D and 3D culture, which subsequently differentiate into self-organized nephron-like structures containing glomeruli, proximal tubules, loops of Henle and distal tubules in a contiguous, ordered arrangement analogous to that of nephrons. To our knowledge, no previous study has converted hPSCs into nephron structures with mature contiguous, ordered segments. Others¹⁸ have generated

SIX2⁺ cells, with an efficiency of 20%, that formed 3D aggregates containing isolated tubular structures but not continuous nephron structures with all epithelial components. Moreover, the protocol generated cells of both the metanephric mesenchyme and ureteric bud lineages, suggesting a lack of specificity. In comparison, our method generates SIX2⁺SALL1⁺WT1⁺PAX2⁺ NPCs with 90% efficiency, and the cells spontaneously give rise to nephron structures containing all the major epithelial derivatives of the metanephric mesenchyme without detectable ureteric bud derivatives. Induction of SIX2⁺ cells from posterior intermediate mesoderm in our protocol required very low doses of FGF9 (10 ng/ml) compared to a concentration 20 times higher in the earlier study¹⁸, suggesting that the WT1⁺HOXD11⁺ posterior intermediate mesoderm cells are primed to respond to FGF9 and differentiate into NPCs. Taguchi and colleagues introduced the concept that targeting axial stem cells and posterior intermediate mesoderm could facilitate the derivation of NPCs of the metanephric mesenchyme^{17,48}. Their protocol, based on an embryoid body culture system, required more intermediate steps and growth factors at each step and used mouse embryonic spinal cord to induce NPCs to undergo tubulogenesis. In addition, the persistent

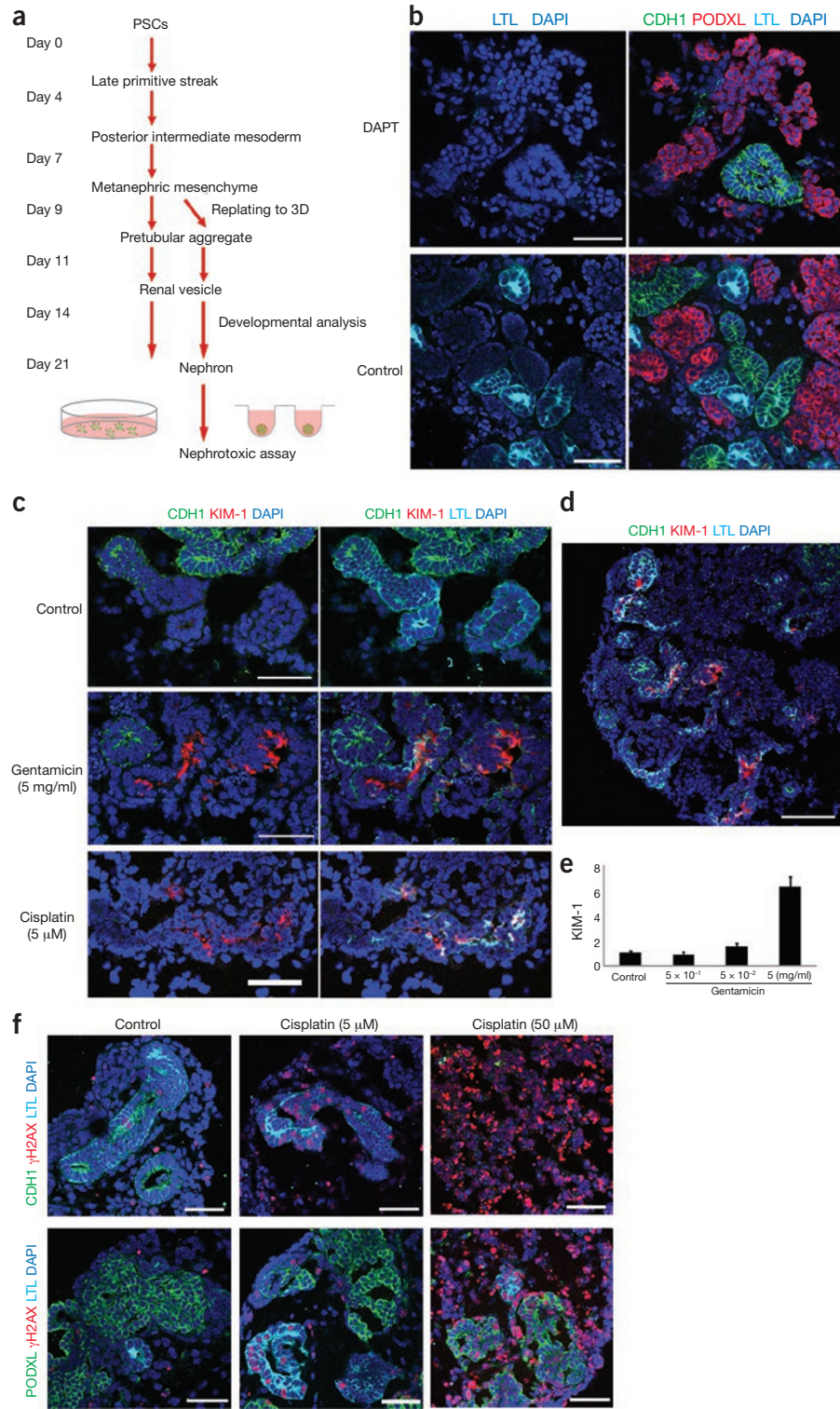


Figure 6 Modeling kidney development and injury in kidney organoids. **(a)** Schematic for kidney development analysis and nephrotoxicity assay. **(b)** Representative images of immunohistochemistry in structures derived from hESCs treated with DAPT 10 μ M from day 14 to 21. $n = 4$. Notch inhibition suppressed proximal tubule formation. Scale bars, 50 μ m. **(c)** Representative immunohistochemistry in structures treated with gentamicin (5 mg/ml) from day 21 to 23 or cisplatin (5 μ M) from day 21 to 22. $n = 6$. Scale bars, 50 μ m. Gentamicin and cisplatin induced the upregulation of KIM-1, and cisplatin suppressed CDH1 expression. **(d)** A low-magnification image of gentamicin-treated organoids. Scale bar, 100 μ m. **(e)** Real-time quantitative PCR of KIM-1 in kidney organoids treated with gentamicin at indicated doses. Data are expressed as mean \pm s.e.m. ($n = 10$). **(f)** Representative immunohistochemistry of organoids treated with cisplatin (5 or 50 μ M) from day 23 to 24 (24 h). $n = 4$. Scale bars, 50 μ m.

expression of SALL1 in the tubular structures indicated that they were still at an immature stage of nephron development. Our protocol to generate posterior intermediate mesoderm and NPCs uses 2D monolayer culture, fewer steps, fewer chemicals and is fully chemically defined and more rapid. A key difference between our protocol and previous ones^{17,18} is our strategy to induce late-stage mid-primitive streak rather than posterior primitive streak, based on developmental studies showing that the posterior primitive streak gives rise to lateral plate mesoderm rather than intermediate mesoderm^{24–26}. By precisely defining the appropriate anterior-posterior position within the primitive streak (with the dose of CHIR and suppression of BMP4) and the timing of cell migration out of the primitive streak (with the duration of CHIR treatment), we could generate the correct precursor population that would give rise to NPCs. As predicted, posteriorization of the primitive streak with the addition of BMP4 causes hPSCs to differentiate into FOXF1⁺ lateral plate mesoderm. Finally, we show that minor modifications in the protocol optimize the efficiency of directed differentiation in both hESC and hiPSC lines. Variability in the levels of endogenous BMP4 signaling markedly affected our ability to differentiate an hiPSC line into posterior intermediate mesoderm, but this could be addressed by adjusting BMP4 levels with the addition of the antagonist noggin.

As shown in previous studies in which hPSCs are differentiated to other lineages, we find that closely recapitulating critical developmental stages *in vitro* improves differentiation efficiencies and produces cells that most closely resemble their *in vivo* counterparts. Our hPSC-derived NPCs express all of the markers of metanephric mesenchyme and possess the intrinsic ability to spontaneously differentiate into renal vesicles and nephrons. Although the absence of ureteric bud and vascular progenitors in our system precludes the generation of collecting ducts and glomerular capillaries, respectively, the NPC-derived renal vesicles self-organize into nephrons without these components in both 2D and 3D contexts.

The ability to generate 3D kidney organoids will facilitate studies of kidney development, disease and injury and of cell replacement therapies. Similar organoid systems have shown promising results for modeling the brain and gastric symptoms^{49,50}. Our data demonstrating that Notch inhibition suppresses proximal tubular differentiation confirm the utility of our system for studying mechanisms of human kidney development, for which no models currently exist. Using gentamicin and cisplatin, we have also shown how the presence of the major epithelial components of the nephron in the

organoids allows screening for toxic drug effects on multiple nephron segments. Given the individual variation in drug sensitivity in humans, the generation of kidney organoids from human iPSCs would enable drug testing in a patient-specific manner.

METHODS

Methods and any associated references are available in the [online version of the paper](#).

Note: Any *Supplementary Information* and *Source Data* files are available in the [online version of the paper](#).

ACKNOWLEDGMENTS

The authors thank V. Bijol for providing electron microscopy images of normal human kidneys, L. Racusen (Johns Hopkins Hospital) for HKC-8, J. Barasch (Columbia University) for a mouse ureteric bud cell line, and A.P. McMahon (University of Southern California) for NIH3T3-Wnt4. This study was supported by US National Institutes of Health (NIH) grants R37 DK039773 and R01 DK072381 (J.V.B.); Grant-in-Aid for JSPS (Japan Society for the Promotion of Science); Postdoctoral Fellowship for Research Abroad (R.M.); American Heart Association grant 11FTF7320023 (A.Q.L.); Harvard Stem Cell Institute (A.Q.L., J.V.B. and M.T.V.); and NIH DK102826 and National Kidney Foundation Young Investigator Grant (B.S.F.).

AUTHOR CONTRIBUTIONS

R.M. and J.V.B. formulated the strategy for this study. R.M. designed and performed experiments. R.M., A.Q.L. and J.V.B. wrote the manuscript. A.Q.L. and B.S.F. performed nephrotoxicity assays. S.K. performed real-time PCR. M.T.V. and J.V.B. helped to design experiments. All authors helped to interpret the results.

COMPETING FINANCIAL INTERESTS

The authors declare competing financial interests: details are available in the [online version of the paper](#).

Reprints and permissions information is available online at <http://www.nature.com/reprints/index.html>.

1. Coresh, J. *et al.* Prevalence of chronic kidney disease in the United States. *J. Am. Med. Assoc.* **298**, 2038–2047 (2007).
2. Herzlinger, D., Koseki, C., Mikawa, T. & al-Awqati, Q. Metanephric mesenchyme contains multipotent stem cells whose fate is restricted after induction. *Development* **114**, 565–572 (1992).
3. Self, M. *et al.* Six2 is required for suppression of nephrogenesis and progenitor renewal in the developing kidney. *EMBO J.* **25**, 5214–5228 (2006).
4. Kobayashi, A. *et al.* Six2 defines and regulates a multipotent self-renewing nephron progenitor population throughout mammalian kidney development. *Cell Stem Cell* **3**, 169–181 (2008).
5. Boyle, S. *et al.* Fate mapping using Cited1-CreERT2 mice demonstrates that the cap mesenchyme contains self-renewing progenitor cells and gives rise exclusively to nephronic epithelia. *Dev. Biol.* **313**, 234–245 (2008).
6. Hinchliffe, S.A., Sargent, P.H., Howard, C.V., Chan, Y.F. & van Velzen, D. Human intrauterine renal growth expressed in absolute number of glomeruli assessed by the disector method and Cavalieri principle. *Lab. Invest.* **64**, 777–784 (1991).
7. Humphreys, B.D. *et al.* Intrinsic epithelial cells repair the kidney after injury. *Cell Stem Cell* **2**, 284–291 (2008).
8. Georgas, K.M., Chiu, H.S., Lesieur, E., Rumballe, B.A. & Little, M.H. Expression of metanephric nephron-patterning genes in differentiating mesonephric tubules. *Dev. Dyn.* **240**, 1600–1612 (2011).
9. Kim, D. & Dressler, G.R. Nephrogenic factors promote differentiation of mouse embryonic stem cells into renal epithelia. *J. Am. Soc. Nephrol.* **16**, 3527–3534 (2005).
10. Vigneau, C. *et al.* Mouse embryonic stem cell-derived embryoid bodies generate progenitors that integrate long term into renal proximal tubules *in vivo*. *J. Am. Soc. Nephrol.* **18**, 1709–1720 (2007).
11. Morizane, R., Monkawa, T. & Itoh, H. Differentiation of murine embryonic stem and induced pluripotent stem cells to renal lineage *in vitro*. *Biochem. Biophys. Res. Commun.* **390**, 1334–1339 (2009).
12. Narayanan, K. *et al.* Human embryonic stem cells differentiate into functional renal proximal tubular-like cells. *Kidney Int.* **83**, 593–603 (2013).
13. Morizane, R. *et al.* Kidney specific protein-positive cells derived from embryonic stem cells reproduce tubular structures *in vitro* and differentiate into renal tubular cells. *PLoS One* **8**, e64843 (2014).
14. Mae, S. *et al.* Monitoring and robust induction of nephrogenic intermediate mesoderm from human pluripotent stem cells. *Nat. Commun.* **4**, 1367 (2013).
15. Xia, Y. *et al.* Directed differentiation of human pluripotent cells to ureteric bud kidney progenitor-like cells. *Nat. Cell Biol.* **15**, 1507–1515 (2013).
16. Lam, A.Q., Freedman, B.S. & Bonventre, J.V. Directed differentiation of pluripotent stem cells to kidney cells. *Semin. Nephrol.* **34**, 445–461 (2014).
17. Taguchi, A. *et al.* Redefining the *in vivo* origin of metanephric nephron progenitors enables generation of complex kidney structures from pluripotent stem cells. *Cell Stem Cell* **14**, 53–67 (2014).
18. Takasato, M. *et al.* Directing human embryonic stem cell differentiation towards a renal lineage generates a self-organizing kidney. *Nat. Cell Biol.* **16**, 118–126 (2014).
19. Kang, M. & Han, Y.M. Differentiation of human pluripotent stem cells into nephron progenitor cells in a serum and feeder free system. *PLoS One* **9**, e94888 (2014).
20. Lam, A.Q. *et al.* Rapid and efficient differentiation of human pluripotent stem cells into intermediate mesoderm that forms tubules expressing kidney proximal tubular markers. *J. Am. Soc. Nephrol.* **25**, 1211–1225 (2014).
21. Imberti, B. *et al.* Renal progenitors derived from human iPSCs engraft and restore function in a mouse model of acute kidney injury. *Sci. Rep.* **5**, 8826 (2015).
22. Grote, D., Souabni, A., Busslinger, M. & Bouchard, M. Pax 2/8-regulated Gata 3 expression is necessary for morphogenesis and guidance of the nephric duct in the developing kidney. *Development* **133**, 53–61 (2006).
23. Attia, L., Yelin, R. & Schultheiss, T.M. Analysis of nephric duct specification in the avian embryo. *Development* **139**, 4143–4151 (2012).
24. Lengerke, C. *et al.* BMP and Wnt specify hematopoietic fate by activation of the Cdx-Hox pathway. *Cell Stem Cell* **2**, 72–82 (2008).
25. Liu, P. *et al.* Requirement for Wnt3 in vertebrate axis formation. *Nat. Genet.* **22**, 361–365 (1999).
26. Iimura, T. & Pourquié, O. Collinear activation of Hoxb genes during gastrulation is linked to mesoderm cell ingressions. *Nature* **442**, 568–571 (2006).
27. Deschamps, J. & van Nes, J. Developmental regulation of the Hox genes during axial morphogenesis in the mouse. *Development* **132**, 2931–2942 (2005).
28. Osafune, K. *et al.* Marked differences in differentiation propensity among human embryonic stem cell lines. *Nat. Biotechnol.* **26**, 313–315 (2008).
29. Bock, C. *et al.* Reference Maps of human ES and iPS cell variation enable high-throughput characterization of pluripotent cell lines. *Cell* **144**, 439–452 (2011).
30. Mahlapuu, M., Ormestad, M., Enerbäck, S. & Carlsson, P. The forkhead transcription factor Foxf1 is required for differentiation of extra-embryonic and lateral plate mesoderm. *Development* **128**, 155–166 (2001).
31. Zimmerman, L.B., De Jesús-Escobar, J.M. & Harland, R.M. The Spemann organizer signal noggin binds and inactivates bone morphogenetic protein 4. *Cell* **86**, 599–606 (1996).
32. Barak, H. *et al.* FGF9 and FGF20 maintain the stemness of nephron progenitors in mice and man. *Dev. Cell* **22**, 1191–1207 (2012).
33. Narlis, M., Grote, D., Gaitan, Y., Boualia, S.K. & Bouchard, M. Pax2 and pax8 regulate branching morphogenesis and nephron differentiation in the developing kidney. *J. Am. Soc. Nephrol.* **18**, 1121–1129 (2007).
34. Kispert, A., Vainio, S. & McMahon, A.P. Wnt-4 is a mesenchymal signal for epithelial transformation of metanephric mesenchyme in the developing kidney. *Development* **125**, 4225–4234 (1998).
35. Barasch, J., Pressler, L., Connor, J. & Malik, A. A ureteric bud cell line induces nephrogenesis in two steps by two distinct signals. *Am. J. Physiol.* **271**, F50–F61 (1996).
36. Carroll, T.J., Park, J.S., Hayashi, S., Majumdar, A. & McMahon, A.P. Wnt9b plays a central role in the regulation of mesenchymal-to epithelial transitions underlying organogenesis of the mammalian urogenital system. *Dev. Cell* **9**, 283–292 (2005).
37. Potter, S.S., Hartman, H.A., Kwan, K.M., Behringer, R.R. & Patterson, L.T. Laser capture-microarray analysis of Lim1 mutant kidney development. *Genesis* **45**, 432–439 (2007).
38. Park, J.S. *et al.* Six2 and Wnt regularly self-renewal and commitment of nephron progenitors through shared gene regulatory networks. *Dev. Cell* **23**, 637–651 (2012).
39. Nouwen, E.J., Dauwe, S., van der Biest, I. & De Broe, M.E. Stage- and segment-specific expression of cell-adhesion molecules N-CAM, A-CAM, and L-CAM in the kidney. *Kidney Int.* **44**, 147–158 (1993).
40. Nakai, S. *et al.* Crucial roles of Brn1 in distal tubule formation and function in mouse kidney. *Development* **130**, 4751–4759 (2003).
41. Georgas, K. *et al.* Use of dual section mRNA *in situ* hybridisation/immunohistochemistry to clarify gene expression patterns during the early stages of nephron development in the embryo and in the mature nephron of the adult mouse kidney. *Histochem. Cell Biol.* **130**, 927–942 (2008).
42. Georgas, K. *et al.* Analysis of early nephron patterning reveals a role for distal RV proliferation in fusion to the ureteric tip via a cap mesenchyme-derived connecting segment. *Dev. Biol.* **332**, 273–286 (2009).
43. Cheng, H.T. *et al.* Gamma-secretase activity is dispensable for mesenchyme-to-epithelium transition but required for podocyte and proximal tubule formation in developing mouse kidney. *Development* **130**, 5031–5042 (2003).
44. Cheng, H.T. *et al.* Notch2, but not Notch1, is required for proximal fate acquisition in the mammalian nephron. *Development* **134**, 801–811 (2007).
45. Uchino, S. *et al.* Acute renal failure in critically ill patients: a multinational, multicenter study. *J. Am. Med. Assoc.* **294**, 813–818 (2005).
46. Whiting, P.H. & Brown, P.A. The relationship between enzymuria and kidney enzyme activities in experimental gentamicin nephrotoxicity. *Ren. Fail.* **18**, 899–909 (1996).
47. Vaidya, V.S. *et al.* Kidney injury molecule-1 outperforms traditional biomarkers of kidney injury in preclinical biomarker qualification studies. *Nat. Biotechnol.* **28**, 478–485 (2010).
48. Taguchi, A. & Nishinakamura, R. Nephron reconstitution from pluripotent stem cells. *Kidney Int.* **87**, 894–900 (2015).
49. Lancaster, M.A. *et al.* Cerebral organoids model human brain development and microcephaly. *Nature* **501**, 373–379 (2013).
50. McCracken, K.W. *et al.* Modelling human development and disease in pluripotent stem-cell-derived gastric organoids. *Nature* **516**, 400–404 (2014).

ONLINE METHODS

Maintenance of hPSCs. H9 human ESCs (passages 45–65), and HDF- α human iPSCs (hiPSC derived from healthy fibroblasts; passages 22–42) were maintained in ReproFF2 (ReproCELL, #RCHEMD006) supplemented with FGF2 (10 ng/ml) (Peprotech, #100-18B) in 6-well tissue culture plates (Falcon, #353046) coated with 1% vol/vol LDEV-Free hESC-qualified Geltrex (Life Technologies, #A1413302) in a 37 °C incubator with 5% CO₂. hPSCs were passaged using Dissociation Solution for human ESCs/iPSCs (ReproCELL, #RCHETP002) at a 1:3 split ratio every 7 days according to the manufacturer's protocol. H9 was purchased from WiCell. HDF- α human iPSCs were previously established in our laboratory⁵¹.

Differentiation of hPSCs. hPSCs grown on Geltrex were washed once with PBS (Life Technologies, #10010-049) and dissociated into single cells with Accutase (STEMCELL Technologies, #07920). Cells were then plated at a density of 2–2.4 × 10⁴ (H9) or 1–1.4 × 10⁴ (HDF, 2C) cells/cm² onto 24-well tissue culture plates (TPP, #92024) coated with 1% Geltrex in ReproFF2 supplemented with the ROCK inhibitor Y27632 (10 μM) (TOCRIS, #1254) and FGF2 (10 ng/ml). After 72 h, cells (50% confluent) were briefly washed in PBS and then cultured in basic differentiation medium consisting of Advanced RPMI 1640 (Life Technologies, #12633-020) and 1× L-GlutaMAX (Life Technologies, #35050-061) supplemented with CHIR99021 (8–10 μM) (TOCRIS, #4423) for 4 days to induce late primitive streak cells. Noggin (5 ng/ml) was also used for hiPSC differentiation in addition to CHIR (10 μM). To induce posterior intermediate mesoderm, cells were then cultured in Advanced RPMI + 1× L-GlutaMAX + activin (10 ng/ml) (R&D, #338-AC-050) for 3 days. For induction of nephron progenitor cells, the media was then changed to Advanced RPMI + 1× L-GlutaMAX + FGF9 (10 ng/ml) (R&D, #273-F9-025/CF) for 7 days. CHIR (3 μM) was added to the media from day 9 to 11 of differentiation to induce renal vesicles. On day 14, cells were switched to the basic differentiation medium and cultured for an additional 7 to 14 days (total of 21 to 28 days). The medium was replaced every 2 or 3 days. The list of growth factors and small molecules that were tested for differentiation are shown in **Supplementary Table 1**.

3D kidney organoid formation. hPSCs on day 9 of differentiation, which represents metanephric mesenchyme cells, were dissociated with Accutase and resuspended in the basic differentiation medium supplemented with CHIR (3 μM) and FGF9 (10 ng/ml), and placed in 96-well, round bottom, ultra-low-attachment plates (Corning, #7007) at 1 × 10⁵ cells per well. The plates were centrifuged at 1,500 r.p.m. for 15 s, and the cells then cultured at 37 °C, 5% CO₂ for 2 days. The medium was then changed to the basic differentiation medium supplemented with FGF9 10 ng/ml and cultured for 3 more days. After that, the organoids were cultured in basic differentiation medium with no additional factors for 7–21 days (a total of 21–35 days).

Nephrotoxicity assay. 3D kidney organoids were cultured in basic differentiation medium supplemented with gentamicin 5 × 10⁻⁴, 5 × 10⁻² or 5 mg/ml (Sigma, #G1264) for 48 h or cisplatin 5 or 50 μM (Sigma, #P4394) for 2, 6, 24 or 48 h after day 21 of differentiation. Organoids were then fixed with 4% paraformaldehyde (Electron Microscopy Sciences, #RT15710) for 20 min for both whole-mount and frozen section immunohistochemistry.

Immunocytochemistry. Cell cultures were washed once with PBS and fixed in 4% paraformaldehyde for 15 min at room temperature (RT). Fixed cells were washed three times in PBS and incubated in blocking buffer (0.3% Triton X-100 and 5% normal donkey serum) for 1 h at RT. The cells were then incubated with primary antibody overnight at 4 °C or for 2 h at RT in antibody dilution buffer (0.3% Triton X-100 and 1% BSA in PBS). Cells were then washed three times in PBS and incubated with Alexa Fluor 488-, 555- or 647-conjugated secondary antibodies (1:500) (Life Technologies) in antibody dilution buffer for 1 h at RT. For immunostaining with biotinylated LTL (Vector Labs, #B-1325), Streptavidin/Biotin Blocking Kit (Vector Labs, #SP-2002) and Alexa Fluor 488- or 647-conjugated streptavidin (Lafe Technologies) were used according to manufacturer's instructions. Nuclei were counterstained with DAPI (Sigma, #D8417). A list of primary antibodies is given in **Supplementary Table 2**. Immunofluorescence was visualized using an inverted fluorescence microscope (Nikon Eclipse Ti). Quantification was performed using ImageJ by counting three to five representative fields per

experiment at 20× magnification. The sample number of biological replicates in each experiment is shown in figure legends.

Whole-mount immunohistochemistry of 3D organoids. 3D kidney organoids were fixed with 4% paraformaldehyde in PBS for 20 min at RT in a 96-well plate, then washed three times in PBS. The organoids were then incubated in blocking buffer (0.3% Triton X-100 and 5% normal donkey serum) for 1 h at RT, then washed three times in PBS. The organoids were incubated with primary antibodies in antibody dilution buffer (0.3% Triton X-100 and 1% BSA in PBS) overnight at 4 °C. The organoids were then washed with PBS three times for 1 h each, with the third washing performed overnight at 4 °C. For immunostaining with biotinylated LTL (Vector Labs, #B-1325), a Streptavidin/Biotin Blocking Kit (Vector Labs, #SP-2002) was used according to the manufacturer's protocol. The organoids were incubated with secondary antibodies in antibody dilution buffer for 1 h at RT, then washed with PBS three times for 30 min each. Nuclei were counterstained with DAPI for more than 30 min. The organoids were then mounted with Vectashield (Vector Labs, #H-1200) and examined by confocal microscopy (Nikon C1, Tokyo, Japan).

Immunohistochemistry of 3D organoids. 3D kidney organoids were fixed with 4% paraformaldehyde in PBS for 20 min in a 96-well plate, washed three times in PBS, then incubated with 30% sucrose (w/w) overnight at 4 °C. The organoids were mounted with O.C.T. compound (Fisher Scientific, #23-730-571) to make frozen blocks and were cut into 10-μm sections. The sections were washed three times in PBS for 5 min each, then incubated in blocking buffer (0.3% Triton X-100 and 5% normal donkey serum) for 1 h. The sections were incubated with primary antibodies in antibody dilution buffer (0.3% Triton X-100 and 1% BSA in PBS) for 2 h, then washed three times in PBS. The sections were incubated with secondary antibodies in antibody dilution buffer for 1 h, then washed three times in PBS. The sections were then treated with Vectashield with DAPI. Imaging was performed with a Nikon C1 confocal microscope.

Quantitative RT-PCR. Total RNA was purified from cells using the RNAeasy MiniKit (Qiagen). 500 ng of RNA was used for reverse transcription with High-Capacity cDNA Reverse Transcription Kit (Life Technologies, #4368814) according to the manufacturer's protocol. RT-PCR reactions were run in duplicate using cDNA (diluted 1:10), 300 nM forward and reverse primers, and iTAQ SYBR Green Supermix (Bio-Rad, #172-5122). Quantitative RT-PCR was performed using the iQ5 Multicolor Real-Time PCR Detection System (Bio-Rad). All samples were run with two technical replicates. β-actin was used as the housekeeping gene. Values were calculated by the delta delta Ct method. Primer sequences are listed in **Supplementary Table 3**.

Flow cytometry. Cells were dissociated using Accutase for 10 min, and cell clumps were removed with a 40-μm cell strainer (Corning, #352340). Cells were fixed with 2% paraformaldehyde for 15 min on ice and then permeabilized with 0.1% Triton for 15 min on ice. Cells were then blocked with PBS + 5% donkey serum for 15 min and incubated with primary antibodies (PAX8 1:2,500, LHX1 1:100, SIX2 1:1,000, SALL1 1:100, WT1 1:100) for 30 min. After washing three times with 1% BSA in PBS, cells were incubated with secondary antibodies (Alexa Fluor 488-conjugated donkey anti-rabbit 1:5,000 (Life Technologies), Cy5-conjugated donkey anti-mouse 1:2,500 (Jackson ImmunoResearch) or Alexa Fluor 647-conjugated donkey anti-mouse 1:5,000 (Life Technologies)) for 20 min on ice. Cells were then washed three times with 1% BSA in PBS. Flow cytometry was performed using MACSQuant (Miltenyi Biotec). Optimal dilution ratios of antibodies were determined using negative controls, undifferentiated H9 and human proximal tubular cell line (HCK-8) that does not express PAX8, LHX1, SIX2, SALL1 or WT1. HCK-8 was kindly provided by Lorraine Racusen (Johns Hopkins Hospital).

Transmission electron microscopy. 3D kidney organoids were fixed with 4% PFA for 20 min and subsequently fixed with electron microscopy (EM) fixation buffer consisting of 1.5% glutaraldehyde, 1% paraformaldehyde, 70 mM NaPO₄ pH 7.2 and 3% sucrose in water overnight at 4 °C. The organoids were washed three times in 0.2 M cacodylate buffer pH 7.4 for 10 min each and were incubated with 1% OsO₄ for 1 h on ice. The organoids were then washed three times in 0.2 M cacodylate buffer pH 7.4 for 10 min each, dehydrated through

a graded series of ethanol solutions, and embedded in Epon. 70 nm sections were cut and analyzed on a JEM-1010 (JEOL).

Cell culture. HKC-8 was maintained in DMEM/F12 (Life Technologies, #11320-033) supplemented with 10% FBS (FBS) in a 37 °C incubator with 5% CO₂ and was passaged every 3 or 4 days. NIH3T3-Wnt4 was maintained in DMEM (Corning, #10-013-CV) supplemented with 10% FBS in a 37 °C incubator with 5% CO₂ and was passaged every 3 or 4 days. NIH3T3-Wnt4 was kindly pro-

vided by Andrew P. McMahon. A mouse ureteric bud cell line was maintained in DMEM (Corning, #10-013-CV) supplemented with 10% FBS in a 37 °C incubator with 5% CO₂ and was passaged every 3 or 4 days. A mouse ureteric bud cell line was kindly provided by Jonathan Barasch. Mycoplasma contamination was tested by DAPI staining in all cell lines.

51. Freedman, B.S. *et al.* Reduced ciliary polycystin-2 in induced pluripotent stem cells from polycystic kidney disease patients with PKD1 mutations. *J. Am. Soc. Nephrol.* **24**, 1571–1586 (2013).